IOP Conf. Series: Materials Science and Engineering **330** (2018) 012010 doi:10.1088/1757-899X/330/1/012010

Effect of ca^{+2} addition on the properties of $ce_{0.8}gd_{0.2}o_{2-\delta}$ for it-sofc

Koteswararao P[1*], M Buchi Suresh[2], B N Wani[3], P V Bhaskara Rao[4] and P.Varalaxmi[5]

[1]Department of physics, Institute of Aeronautical engineering college, Dundigal, Hyderabad, Telangana, India
[2]Center for Ceramic Processing, International Advanced Research Centre for Powder Metallurgy and New Materials (ARCI), Hyderabad-500005, AP, India.
[3]Chemistry Division, Bhabha Atomic Research Centre, Trombay, Mumbai, India
[4]Department of physics, St. Mary's Engineering College, Deshmukhi, R.R (DT), India
[5]Department of physics, Anurag engineering college, Hyderabad, Telangana, India

*Corresponding author E-mail: koteswarphysics@gmail.com

Abstract. This paper reports the effect of Ca^{2+} addition on the structural and electrical properties of $Ce_{0.8}Gd_{0.2}O_{2-\delta}$(GDC) electrolyte for low temperature solid oxide fuel cell application. The Ca (0, 0.5, 1 and 2 mol %) doped GDC solid electrolytes have been prepared by solid state method. The sintered densities of the samples are greater than 95%. XRD study reveals the cubic fluorite structure. The microstructure of the samples sintered at 1400^{o}C resulted into grain sizes in the range of 1.72 to 10.20 μm. Raman spectra show the presence of GDC single phase. AC impedance analysis is used to measure the ionic conductivity of the electrolyte. Among all the compositions, the highest conductivity is observed in the GDC sample with 0.5 mol% Ca addition. Nyquist plots resulted in multiple redoxation process such as grain and grain boundary conductions to final conductivity. Estimated blocking factor is lower for the GDC electrolyte with 0.5mol% Ca, indicating that Ca addition was promoted grain boundary conduction. Activation energies were calculated from Arrhenius plot and are found in the range of 1eV.

1. Introduction

In recent years doped ceria electrolytes have been attracted a great interest because of their potential as a solid electrolyte for intermediate temperature solid oxide fuel cells (IT-SOFCs) application [1]. In CeO_2 based electrolytes, temperature facilitates movement of oxygen ions through oxygen vacancies which are produced in the oxygen sub-lattice to neutralize the deficiency of charge created by lower valent dopant cations. Doped ceria show higher ionic conductivity at relatively low temperatures (500–700°C) as compared with yttria-stabilized zirconia (8YSZ). Ceria based materials have been extensively studied as the most promising electrolyte materials for IT-SOFCs. In the IT- and LT-regions, the grain-boundaries are ∼102–105 times more resistive than the grain-interior due to space charge layer and siliceous inter-granular phase around the grain boundary. A positively charged grain-boundary core is formed in pure GDC materials due to the different formation energies of individual defects, which lead to the depletion of oxygen vacancies and the accumulation of acceptors near the grain boundary area. On the other hand, even a few hundred ppm of a siliceous impurity can increase he grain-boundary resistivity of GDC up-to 100 times [2-5]. An improvement in grain-boundary conduction is essential to increase the energy-converting efficiency of LT- and IT-SOFCs. Lane et al. [6] reported that grain-boundary conduction can be enhanced substantially by adding CaO and SrO due to the solubility of CaO in GDC is expected to be relatively high due to the ionic radius of Ca2+ (1.12A˚) at a coordination

number of 8 is similar to those of Gd^{3+} (1.06A˚) and Ce^{4+} (0.97A˚). This indicates that the optimum doping concentration for effective scavenging and the scavenging mechanism will be different on doping with CaO [7]. In recent years, researchers have been concentrating on improving the conductivity of electrolytes by co-doping method and this method was found to be effective [8,9]. The co-doping could enhance the ionic conductivity. Dopant ion, dopant concentration, oxygen vacancy concentration and defect association energy and local defect structure are the factors, which can influence the total ionic conductivity in doped ceria. A large number of co doped ceria electrolyte materials have been investigated, such as $Ce_{1-x-y}Gd_xPr_yO_{2-z}$ [10], $Ce_{1-x-}Y_ySm_xLa_yO_{2-z}$ [11], and $Ce_{1-x-y-z}Gd_xSm_yY_zO_{2-d}$ [12]. In the present work, we have selected divalent (Ca^{2+}) and trivalent (Gd^{3+}) as co-dopants because their effective ionic radii are closer to critical radius (r_c).The ionic radius of Ca^{2+} (1.12A˚) at a coordination number of 8 is similar to those of Gd^{3+}(1.06A˚) and Ce^{4+}(0.97A˚). This indicates that the optimum doping concentration for effective scavenging and the scavenging mechanism will both be different on doping with CaO. Gd^{3+} and Ca^{2+} co-doped ceria based materials $Ce_{0.8-x}Gd_{0.2}Ca_xO_{2-\delta}$ (where x =0, 0.005,0.01,0.02) are prepared and characterized. The main aim is to correlate the structure, morphology and ionic conductivity of Ca doped GDC.

2. Experimental

GDC (99.9% purity, 40nm particle size) and CaCO3 (AR grade Sigma Aldrich USA, 99.9% purity) were used as starting materials. The powders of GDC and $CaCO_3$ were mixed in required stoichiometric proportion (0.5, 1 and 2 mol% of $CaCO_3$). The mixture was ground in agate and mortar for 2 hours and calcined at 800ºC for 2 hours. 2wt% of polyvinylpyrrolidone was added to the powder as binder and was mixed thoroughly. All the samples were uniaxially pressed to obtain a disc shaped pellets and sintered at 1400ºC for 2 hours. The synthesized pellets were characterized using X-ray diffraction (Philips X-ray diffactometer), Scanning Electron Microscopy (ZEISS EVO® series SEM),AC Impedance analyzer(Solatron impedance analyzer)

3. Results and discussion

3.1 XRD analysis

Fig.1 shows XRD patterns of Ca^{2+} doped GDC electrolytes [$Ce_{0.8-x}Gd_{0.2}Ca_{0.2}O_{2-\delta}$(x=0,0.5,1,2mol%)]. These patterns confirm that all the compositions show single phase cubic fluorite structure with space group *Fm3m* (JCPDS No 34-0394) [13].

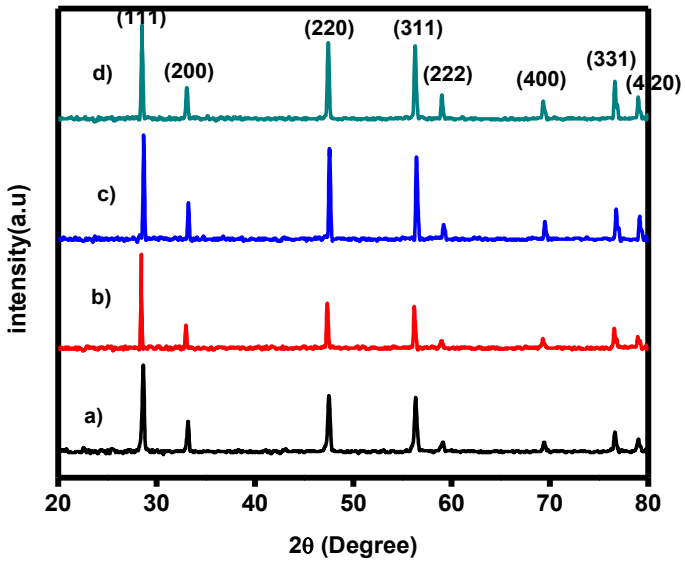

Fig. 1 XRD patterns of (a) GDC and (b) 0.5, (c) 1, and (d) 2 mol % Ca doped GDC samples

Further it is observed that addition of Ca in GDC, resulted in the peak shift to lower 2θ values, which is due to the size of the Ca^{2+} (r=1.12Å) is greater than ceria (0.97 Å) in the unit cell. This results in slight

expansion of the lattice and hence lattice parameter and volume changes, indicating that Ca^{2+} has entered into Ce sites forming a single phase $Ce_{0.8-x}Ca_xGd_{0.2}O_{2-\delta}$[14].

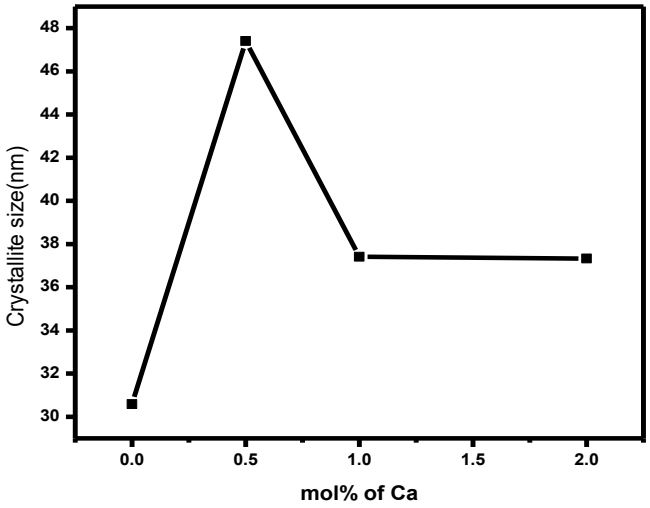

Fig. 2 Variation of Crystallite size with the mol% of Ca in GDC

The variation of crystallite size with mol% is shown in Fig. 2. The crystallite size is observed to increase initially with Ca^{2+} content indicating that Ca^{2+} addition promoted the crystalline growth. Further increase of Ca^{2+}concentration has not effected much on the crystallite size. The densities of all these samples calculated by Archimedes principle are around 95% of the theoretical density.

Table 1 Structural parameters of Ca^{2+} doped GDC samples

Composition	**Lattice Constant (Å)**	**Structure**	**Density (%TD)**
Pure GDC	5.402	Cubic	95
0.5mol% Ca^{2+} doped GDC	5.434	Cubic	96
1mol% Ca^{2+}doped GDC	5.441	Cubic	94.6
2mol% Ca^{2+} doped GDC	5.457	Cubic	95

3.2. Morphological studies

The variation in surface morphologies of sintered pellets of Ca^{2+} doped GDC are shown in Fig 3(a-d). The morphology of all the samples is observed to be compact and homogeneous with the porosity consistent with the measured densities [15].

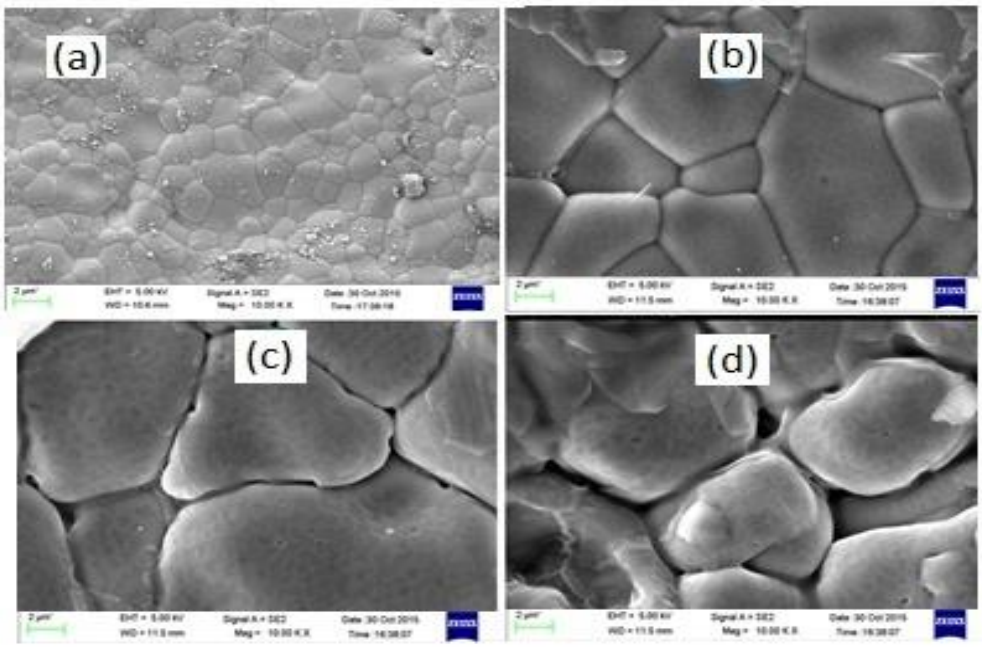

Fig. 3 Surface morphologies of (a) GDC and (b) 0.5, (c) 1, and (d) 2 mol % Ca doped GDC samples

Average grain size of all the samples was calculated by linear intercept method. It is observed that the grain size is increased by increasing Ca^{2+} concentration up to 1 mol% in GDC from 1.72 to 10.20 μm and on further increase of concentration up to 2 mol% has no significant effect on the grain size. The increase in grain sizes with composition up-to 1 mol% leads to the creation of more oxygen vacancies to achieve the high conductivity in those samples [16]. It is known that the grain growth of GDC can be promoted by Ca^{2+} ion doping. Hence, the addition of Ca^{2+} ion can also act as an aid for accelerating CeO_2 sintering. The electrolyte with larger grain size is therefore expected to yield better cell performance. The motion of the grain boundary is an important role in the micro structural development of the samples. During the solid-state sintering the very slow grain boundary mobility will delay the sintering process and results in delay in densification of ceramics, while too fast grain boundary mobility will leads to lots of pores trapped in the interior sites of grains and prevents the full densification of the samples [17].

3.3. EDAX

The EDAX spectra shown in Fig 4(a-d) gives the distribution of elements in the composition, and the presence of Ce^{4+}, Gd^{3+}, O and Ca^{2+} in all the compositions. Ce^{4+}, Gd^{3+}, O and Ca^{2+} ions were almost fully dissolved into the CeO_2 matrix, which was confirmed by EDS.

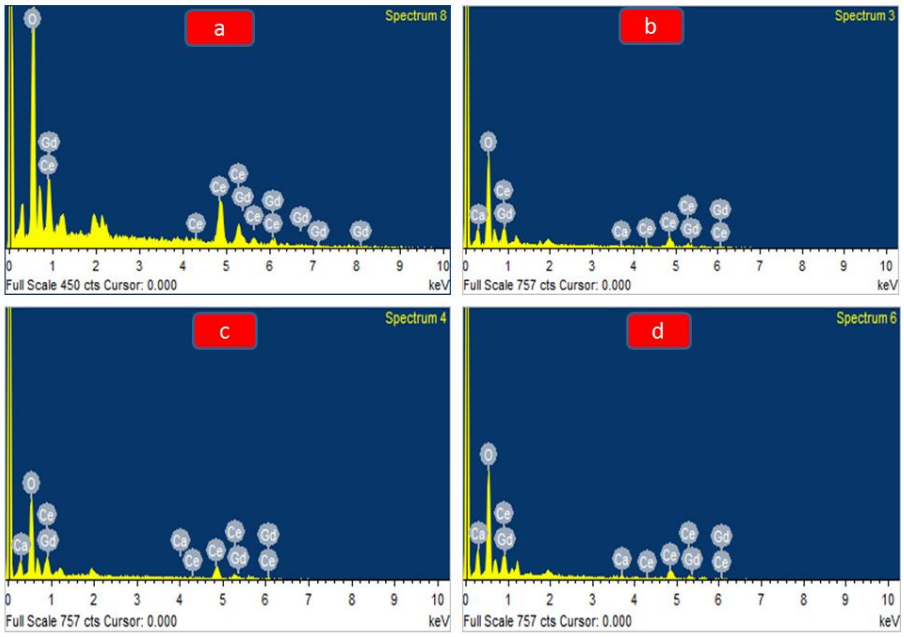

Fig. 4 EDAX spectra of (a) GDC and (b) 0.5, (c) 1, and (d) 2 mol % Ca doped GDC samples

3.4 Raman study

Fig. 5 depicts the Raman spectra of pure and Ca^{2+} co-doped GDC samples sintered at 1400ºC for 2h. A band observed at 471 cm^{-1} corresponds to CeO_2 due to F_{2g} symmetry of the cubic GDC phase [18]. In addition a weak band observed at 550 cm^{-1} corresponds to the defect spaces related to the oxygen vacancies present in the structure of GDC.

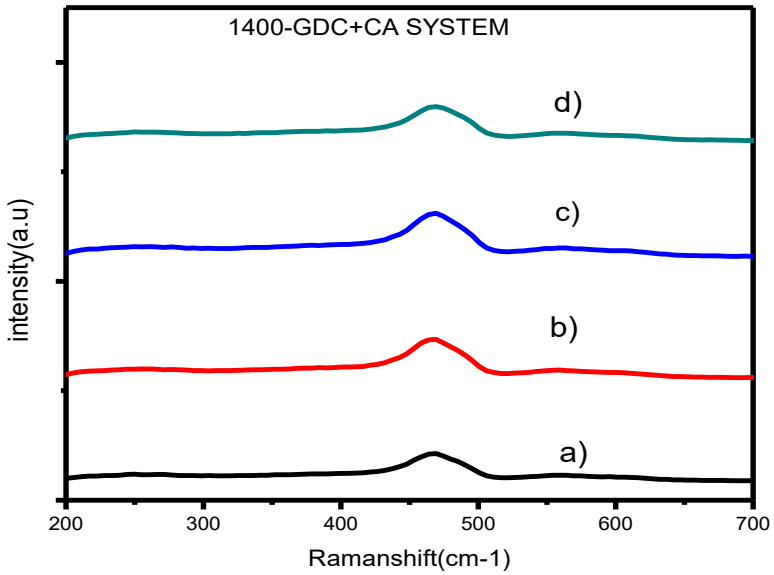

Fig: 5. Raman spectra of (a) GDC, (b) 0.5, (c) 1 and (d) 2 mol % Ca^{2+} doped GDC samples

3.5 Electrical properties

In cerium oxide (CeO_2) vacancies may be introduced by ceria reduction or by doping with oxides of metals of lower valence. These equations are written in KrÖger-Vink notation [19].

$$CaO \xrightarrow{CeO_2} Ca'_{Ce} + O_O^x + V_O^{oo} \text{ ----------} \quad (1)$$

$$Gd_2O_3 \xrightarrow{CeO_2} 2Gd'_{Ce} + 3O_O^x + V_O^{oo}O_O^x + 2Ce_{ce^x} \rightarrow 2Ce_{ce'} + {}^1/_2\, O_{2(gas)} + V_O^{oo} \quad (2)$$

The co-doping of gadolinium (Gd) and calcium (Ca) into cerium oxide (CeO_2) would create oxygen vacancies at low dopant concentration. Cole-Cole plots of pure GDC and Ca doped GDC samples recorded at different temperatures are shown in Fig. 6 to 9. All the plots resulted into two semicircular arcs. The arc in the high frequency is for grain contribution and the arc in the mid and low frequency region is for grain boundary and electrode contributions for the total conduction in the material.

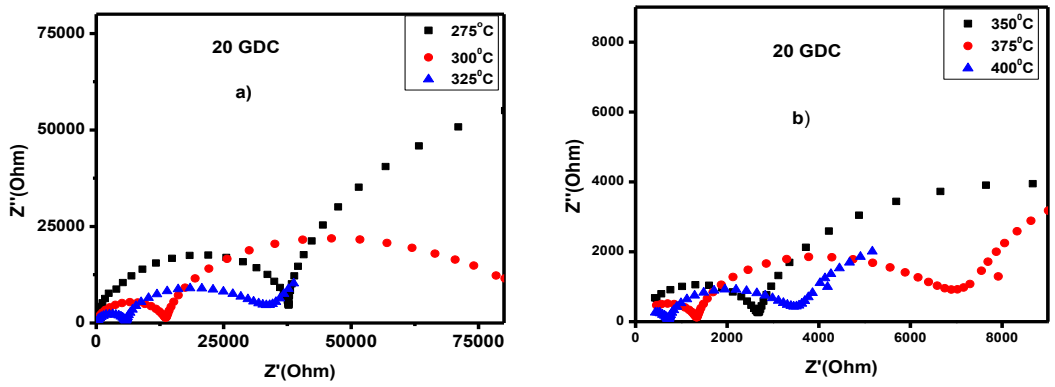

Fig. 6 impedance spectra of GDC at temperatures
a) 275-325 °C b) 350-450 °C

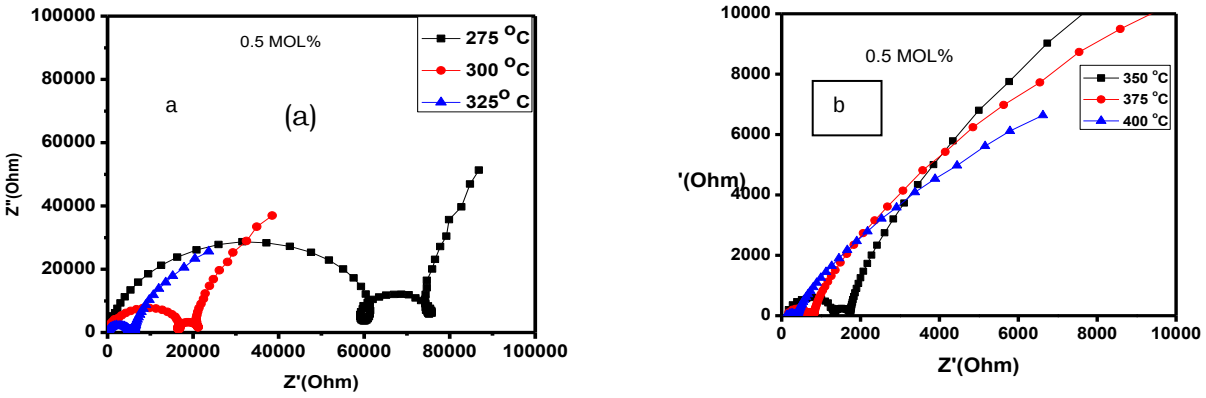

Fig. 7 impedance spectra of 0.5 mol % Ca^{2+} doped GDC at temperatures
a) 275-325 °C b) 350-450 °C

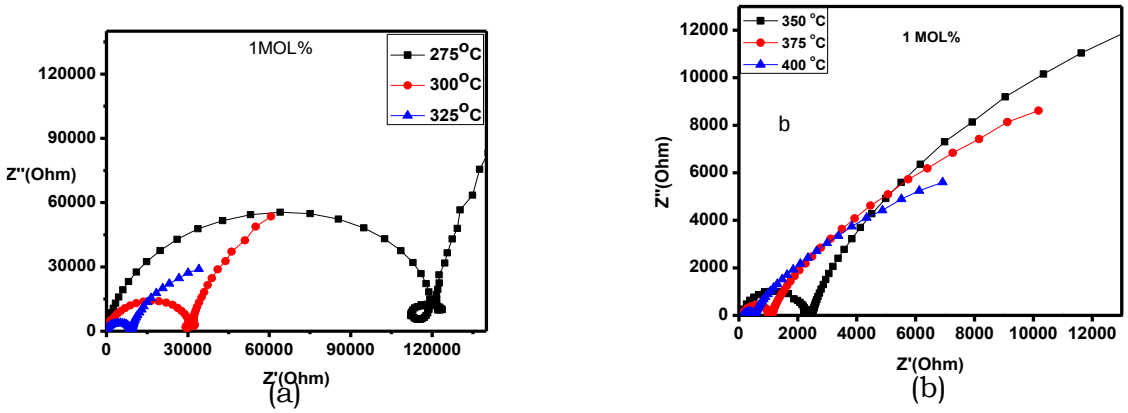

Fig. 8 impedance spectra of 1 mol % Ca^{2+} doped GDC at temperatures a) 275-325 °C b) 350-450 °C

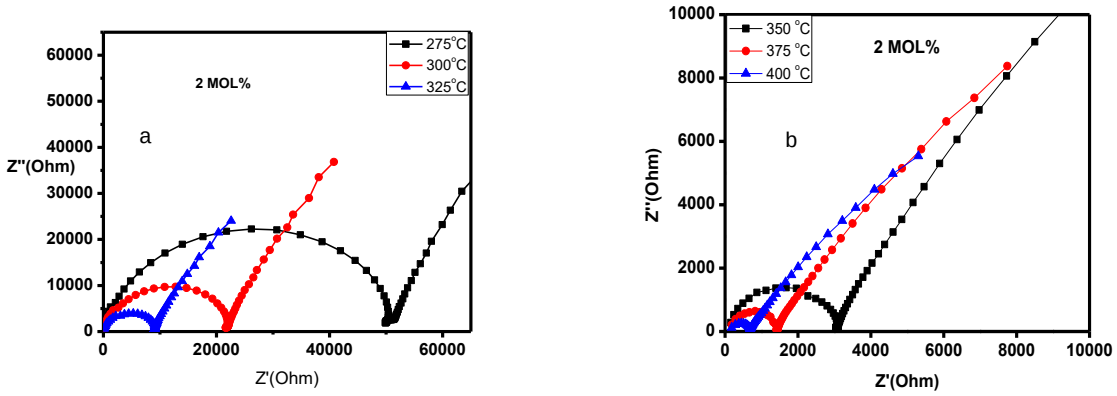

Fig. 9 Impedance spectra of 2 mol % Ca^{2+} doped GDC at temperatures a) 275-325 °C b) 350-400 °C

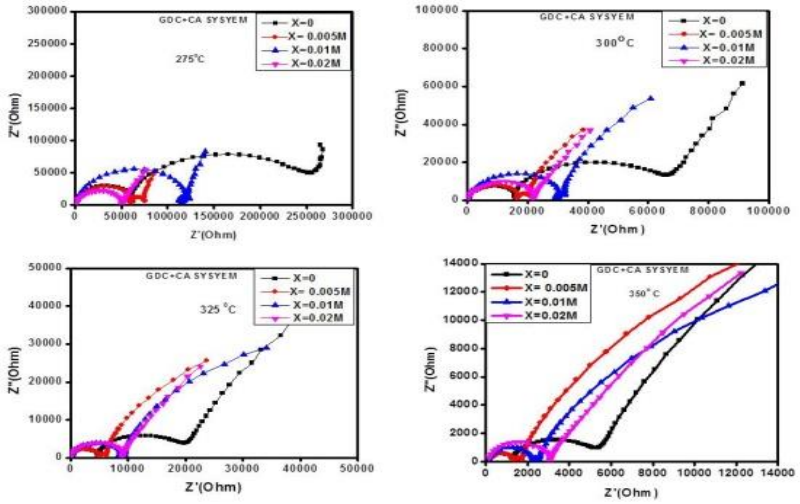

Fig. 10 Cole-Cole plots of (a) GDC and (b) 0.5, (c) 1, and (d) 2 mol % Ca co-doped GDC pellets recorded at 275 °C, 300 °C, 325 °C, 350 °C

The spectrum show arc at high frequency corresponds to grain interior resistance (R_g), semi-circle at intermediate frequency represents grain boundary resistance (R_{gb}) and tail at low frequency represents electrode contributions. Grain resistance grain boundary resistance and electrode resistance (R_e) can be estimated from their intercepts on real axis. It is observed that the size of bulk and grain

boundary semicircles decreases with an increase of temperature and grain boundary resistance is found to be higher than the grain boundary resistance indicates the conduction mechanism in Ca^{2+} doped GDC is due to grains.

At higher temperatures, the semicircle starts intercepting at high frequency side indicating the role of series resistance in the standard material system. The ionic conductivity of GDC was significantly enhanced by Ca^{2+} addition. This might be due to increase in oxygen ion mobility with increasing temperature.

All these plots show two well-separated arcs and portions of a third at the lower frequencies. These graphs clearly indicate that resistivity values are decreased by increasing temperatures [20]. At higher temperatures, the grain boundary semicircles are shifting towards higher frequency side [21]. Fig.10 the shows comparison of spectra recorded at 275°C, 300°C, 325°C, 350°C for all the Ca^{2+} doped samples. The spectra compares arc at high frequency corresponding to grain interior resistance (R_g), at intermediate frequency represents grain boundary resistance (R_{gb}) and tail at low frequency represents electrode contributions.

The conductivity was then calculated from resistance, thickness *l*, and cross-sectional area *A*, by using the formulae $\sigma = l$ /R*A [22]. The variation of the conductivities at different concentrations of Ca^{2+} is show in the Fig. 11.

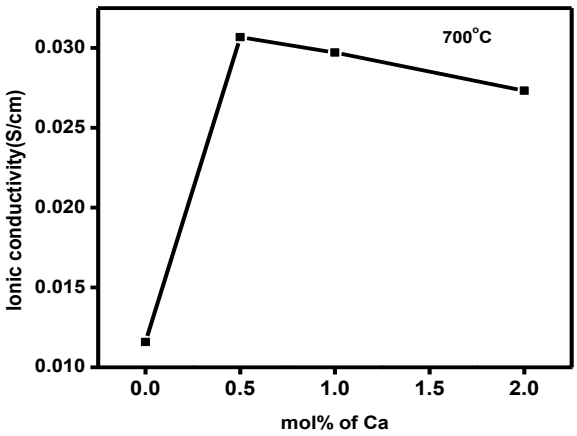

Fig. 11 Variation of conductivity with doping concentration

Conductivity of pure GDC is 0.012 Scm^{-1} at 700°C.With the addition of Ca^{2+}, conductivity increased initially to a maximum value of 0.032 Scm^{-1} and then decreased. It has been observed that highest conductivity is obtained in 0.5mol% Ca^{2+} doped GDC sample. Significant increase in ionic conductivity by addition of Ca^{2+} in GDC might be due to enhancement in the number of oxygen vacancies, with Ca^{2+} acting as grain boundary scavenger, in addition to oxygen vacancy radius and decrease in average binding energy than pure GDC .However, higher the Ca^{2+} concentration, the total conductivity decreases due to defect association leads to lowering of the effective concentration of oxygen vacancies and their mobility. Hence increase in Ca^{2+} content to high values leads to decrease in the overall conductivity.

The fact is attributed to the presence of impurities located in grain boundary, which lowering the ionic mobility. This may be overcome by decreasing grain boundary resistivity *ie.*, lowering the grain boundary density or the substitution of a controlled amount of dopants like MgO, CaO, and $SrCO_3$ which could cleanse the grain boundary of non-adequate impurities in GDC. It is interesting here to compare the processing conditions and the conductivity data reported for $Ce_{0.8}Sm_{0.2}O_{1.9}$ by other workers. Yahiro et al. reported a conductivity of 9.5×10^{-2} Scm^{-1} at 800°C for the 1650°C sintered samples [23]. Huang *etal.*, on the other hand, although they were successful in reducing the sintering

temperature, could observe a conductivity of only 5 ×10^{-3} S cm^{-1} in air at 600°C [24]. On the contrary, Balazs and Glass reported a maximum conductivity of 1.2 × 10^{-2} S cm^{-1} at 600°C for the 1550°C sintered sample [25]. Recently Li et al., reported a reference value of 0.038 S cm^{-1} at 700°C for the $Ce_{0.8}Sm_{0.2}O_{1.9}$ composition sintered at 1200°C [26]. In comparison to the above literature on the sintering and conductivity of the $Ce_{0.8-x}Gd_{0.2}Ca_xO_{2-\delta}$ composition, the Ca^{2+} doped GDC samples were prepared in the present work could be sintered to a density of more than 90% of theoretical density at 1400°C, and Ca^{2+} doped GDC (0.5mol %) exhibited a conductivity of 0.032 Scm^{-1} at 600°C in air.

3.6. Blocking factor

To validate the foraging result of Ca^{2+} for grain boundary conduction, the manipulation of the grain boundary conduction to the entire conductivity is estimated with the help of the blocking factor (α_R) [27] (α_R) defined as:

$$\alpha_R = Rg/(Rg+Rgb) \quad \text{----------(3)}$$

where, R_g and $R_{gb}$are grain and grain boundary resistances, respectively. This feature affects the electric transport that is obstructed at the non-porous inside areas in terms of the total number of electric carriers in the sample. The lowest blocking factor was examined in 0.5 mol % Ca^{2+}-doped GDC sample *ie.*,0.1173 at 700°C than pure GDC (0.782).

This result clearly demonstrates that Ca^{2+} is an effective scavenger of grain boundary and suggests that the addition of Ca^{2+} promotes the grain boundary conduction and hence the total conduction in GDC. Table 3 gives the activation energies of all the compositions.

Table 2: Table for Activation energies of Ca doped GDC system

COMPOSITION	**Activation Energy(eV)**
Pure GDC	1.25
0.5mol% Ca^{2+} doped GDC	1.1
1 mol% Ca^{2+} doped GDC	1.0
2 mol% Ca^{2+} doped GDC	1

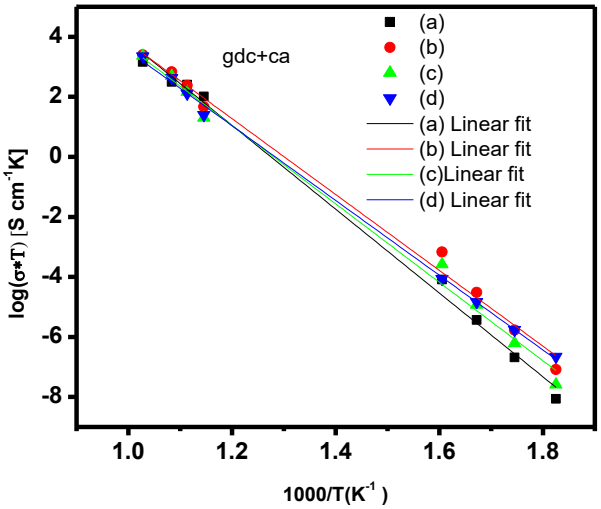

Fig. 12 Arrhenius plots of (a) GDC and (b) 0.5, (c) 1, and (d) 2 mol % Ca doped GDC samples

For a specific composition, with rise in temperature, time constants of both grain and grain boundary processes reduce and corresponding resistances decrease. Hence conductivity rises with the temperature. The temperature dependence of total electrical conductivity (Fig.12) can be fitted into the Arrhenius relation:

$$\sigma = \frac{A}{T}\exp\frac{-Ea}{kT} \quad \text{----------[4]}$$

Fig. 12 shows that the total ionic conductivity increases with increasing Ca^{2+} doping from 0% to 0.5mol% due to more open structure facilitating the movement of the oxide ions leads to increase in the ionic conductivity and thereafter it decreases due to excess positive surface charge in the grain boundaries and bulk surfaces. The same space charge potential results in the accumulation of electrons and the depletion of oxygen vacancies in the space charge layer, and the ionic conductivity decreased with increasing grain boundary area per unit mass. These values agree with the value of activation energy for movement of oxygen ions reported in the literature on such materials.

For a polycrystalline oxygen-ion electrolyte, the activation energy for total ionic conduction originate from three sources, such as enthalpy of the migration of oxygen ions, the association enthalpy of complex defects and the activation energy for conduction in grain boundaries. Generally, three sources simultaneously dominate the total ionic conductivity. In the case of low temperature range (150–500ºC), the oxygen vacancy, which is associated with the dopant is trapped and the activation energy (Ea) is the sum of association and migration enthalpy and the thermodynamic equilibrium between the free defects (V0••) and the associated pairs (R ce-V0••). While in the high temperature range (500–800°C), the activation energy is equal to migration energy because most of the oxygen vacancies are free to migrate and at high temperatures conductivity is controlled by the charge carrying defects determined by an aliovalent dopant or impurity [28].It is concluded that ceria co-doped with $Ca^{2+}$and Gd^{2+} have conductivity comparable with singly or ceria co-doped with rare earth elements. Use of these materials as solid electrolyte for ITSOFC will reduce the cost dramatically [29].

4 CONCLUSIONS

Ca^{2+} doped GDC solid electrolytes are successfully synthesized by solid state reaction method. The XRD study reveals cubic structure with increase in lattice parameter with Ca^{2+}content in pure GDC electrolyte. It is observed that grain size increases by increasing Ca^{2+} concentration up-to 1 mol% from 1.72 to 10.20 μm. Raman spectra showed the presence of band at 471 cm^{-1} corresponding to CeO_2. The ionic conductivity is high for 0.5 mol% Ca^{2+} doped GDC electrolyte than pure GDC due to scavenging effect.

References

[1] Inaba, Hand Tagawa, H1996 *Solid State Ionics.* **8** 1
[2] Steele,B.C.H 2000 *Solid State Ionics.* **51** 129
[3] GuoX, Waser and NowickR. 2006 Prog.*Mater. Sci***. 50** 151
[4] Gerhardt, R.;, AS 1986 J Am Ceram Soc.**69** 641
[5] Gerhardt R, Nowick AS, Mochel ME Dumler I1986. *J Am Ceram Soc.* **69** 647
[6] Lane,J.A, Neff, J.L and Chrisitie G.M 2006 *Solid State Ionics.* **177** 1911
[7] Yahiro H,Ohuchi T ,Eguchi K and AraiH 1988 *J. Mater. Sci*. **23** 1036
[8] HerleJ.V,SeneviratneD and McEvoy1999 *Ceram. Soc.* **19** 837
[9] Mori T,Drennan,J Lee,J.-H 2002 *Solid State Ionics.***154/155** 461
[10]Lubke,S and Wiemhofer,H.D1999 *Solid State Ionics*.**117** 229
[11] Yoshida H, Deguchi H and MiuraK 2001 *Solid State Ionics***. 140** 191
[12]Yoshida H,Inagaki T and Ogumi Z *Solid State Ionics.* Vol**. 160** 200
[13] Ramesh S and Upender G 2013 J. *Modern Phy*.**4** 859
[14] Ramesh S and Upender G J. *Modern Phy* 2013,http://dx.doi.org/10.4236/jmp.2013.46116
[15] Arabaci A and Özgün Serin*2015 J.MaterialsEngg.Performance.* **24,** 2730
[16] Yan P, Hu X and *C*hinese2009 *J. Materials Research*. **23** 405
[17] YC,Wu and Lin ,CC 2014 Int *J Hydrogen Energy.* **39** 7988

[18]Phokha S and Pinitsoontorn S 2013 *Nano-Micro Letters* **5** 223
[19] Inaba H and Tagawa,H.1996 **83** 1-16
[20] Gerhardt R and Nowick,A.S 1986 *J. Am. Ceram.Soc.* **69** 641
[21] Li,H ,Xia Cand Meng G 2006 *Acta Mater., 54* 721
[22] Lai W and Haile S M 2005 *J. Am. Ceramic Society.* **89** 2979
[23]YahiroH, Eguchi Y and EguchiK 1988 *J.Appl. Electrochem.***18** 527
[24] Huang W and Shuk P 1997 *Solid State Ionic.* **100** 23
[25] Balazs G.B and Glass, R.S *1995 Solid State Ionis.***76** 155.
[26] Li H, Xia C and Zhu,2006 M, *Acta Mater*.**54** 721
[27] J.M.; Ralph, Ph.D. Thesis,1998 *University of London*
[28] Omer S, Wachsman ED and Nino JC 2008 *Solid State Ionics.***178** 189
[29] Yu-Chuan Wu, Yi-Yao and Liao2016 *international journal of hydrogen energy.* **41** 13591